EARTH SURFACE PROCESSES AND LANDFORMS
Earth Surf. Process. Landforms **34**, 384–397 (2009)

Published online 13 November 2008 in Wiley InterScience
(www.interscience.wiley.com) DOI: 10.1002/esp.1743

Water-worked gravel beds in laboratory flumes – a natural analogue?

James R. Cooper[1]* and Simon J. Tait[2]
[1] Department of Geography, University of Hull, Hull, HU6 7RX, UK
[2] School of Engineering, Design and Technology, University of Bradford, Bradford, BD7 1DP, UK

Received 22 January 2008; Revised 20 June 2008; Accepted 7 July 2008

* Correspondence to: J. R. Cooper, Department of Geography, University of Hull, Cottingham Road, Hull, HU6 7RX, UK. E-mail: J.R.Cooper@hull.ac.uk

ESPL
Earth Surface Processes and Landforms

ABSTRACT: An investigation has been conducted to identify the key parameters that are likely to scale laboratory sediment deposits to the field scale. Two types of bed formation were examined: one where sediment is manually placed and screeded and the second where sediment is fed into a running flume. This later technique created deposits through sequential cycles of sediment transport and deposition. Detailed bed surface topography measurements have been made over a screeded bed and three fed beds. In addition, bulk subsurface porosity and hydraulic conductivity have been measured. By comparing the four beds, results revealed that certain physical properties of the screeded bed were clearly different from those of the fed beds. The screeded bed had a random organization of grains on both the surface and within the subsurface. The fed beds exhibited greater surface and subsurface organization and complexity, and had a number of properties that closely resembled those found for water-worked gravel beds. The surfaces were water-worked and armoured and there was preferential particle orientation and direction of imbrication in the subsurface. This suggested that fed beds are able to simulate, in a simplified manner, both the surface and subsurface properties of established gravel-bed river deposits. The near-bed flow properties were also compared. It revealed that the use of a screeded bed will typically cause an underestimation in the degree of temporal variability in the flow. Furthermore, time-averaged streamwise velocities were found to be randomly organized over the screeded bed but were organized into long streamwise flow structures over the fed beds. It clearly showed that caution should be taken when comparing velocity measurements over screeded beds with water-worked beds, and that the formation of fed beds offers an improved way of investigating intragravel flow and sediment–water interface exchange processes in gravel-bed rivers at a laboratory scale.

KEYWORDS: water-worked gravel beds; sediment feeding; bed surface topography; near-bed flow; laboratory flume

Introduction

In the simulation of gravel-bed river flows in laboratory flumes much attention has been paid to the issue of spatial scaling. The dimensionless parameters governing the flow dynamics in a river are the Reynolds and Froude numbers. Since it is not possible to scale for both the Reynolds and Froude numbers simultaneously, and since gravity forces predominate in free surface flows, in most cases, this simulation involves the use of undistorted Froude-scale modelling (Peakall *et al.*, 1996). To ensure dynamic similitude, the Froude number in the flume model must be identical to that in the field prototype (Parker *et al.*, 2003), as long as the flow remains within the fully turbulent flow regime. The scaling factor is most often determined by the ratio of the width of the flume to the bankfull width of the field prototype. To ensure that the Froude number is scaled correctly, the flow depth and the grain-size of the bed mixture is reduced by a scaling factor and by setting the flume slope equal to that of the field prototype. Therefore, when modelling the gravel-bed of the field prototype, explicit consideration is only usually given to the scaling of the grain-size distribution, and not to creating bed deposits that geometrically scale with those found in a river.

The surface of a natural water-worked gravel bed displays a spatially complex, three-dimensional, structure. This reflects the arrangement of the sediment particles by transport processes which orientate, imbricate, sort and layer the sediment deposits through the continual deposition and reworking as a result of cycles of floods. Therefore any study in a laboratory flume of the near-bed processes occurring in a gravel-bed river must be able to replicate these characteristics of the bed. Commonly in laboratory studies, a simulated river bed has been produced by placing a given depth of randomly mixed sediment on to the base of the flume, which is then scraped level (screeded). If the grain-size distribution is scaled to that of the field prototype this can be deemed acceptable only if the particle arrangement, orientation, packing, spacing and sorting on the bed is similar to that in the river. However, screeded beds are, in essence, a mixture of randomly sorted and loosely packed grains. Therefore, although the surface of the volumetric grain-size distribution might be similar, the statistical distribution of bed surface elevations and streamwise and lateral roughness length-scales

are distinctly different. Clearly, some surface properties of the bed mixture do not faithfully represent those found in the prototype. Any difference in surface roughness properties are likely to be reflected in the properties of the time-averaged flow, turbulence and flow resistance. Therefore, the authors believe that caution is required when utilizing laboratory fluid velocity measurements over screeded beds in order to explain field measurements.

To overcome this problem, a number of studies have created a screeded bed and then water-worked the bed for a period of time or until a static armour has formed on the surface. This is known to produce a surface topography which better reflects that found in gravel-bed rivers (Butler *et al.*, 2001; Aberle and Nikora, 2006) and a degree of surface coarsening relative to the subsurface which is typically observed (Parker *et al.*, 2003). However, the subsurface of these beds still remains a mixture of randomly sorted grains created by their manual placement. Well-established in-channel fluvial gravel deposits are created by sequential cycles of transport and deposition. Although, in some cases rivers change their course during floods creating new channels, and river restoration projects construct new river beds mechanically so that deposits have not necessarily been water-worked. But the sedimentary properties of well-established deposits reflect the sedimentary processes that form them and therefore create heterogeneity at the lithofacies scale. The different lithofacies are characterized by different grain-size distributions, degrees of particle sphericity, sorting, stratification, fabric and texture (Heinz *et al.*, 2003), and as such the subsurface is far from being randomly sorted. Since there are no post-depositional geologic mechanisms which are likely to create these differences in subsurface architecture, the lithofacies reflect the transport and depositional processes (e.g. Heinz *et al.*, 2003; Barrash and Reboulet, 2004; Kostic *et al.*, 2005). For example, poorly sorted gravel lithofacies are thought to be created by the deposition of low-density, tractional bedload sheets because of the nature of its size sorting, the *a*-axis (long axis) of the coarse clasts being typically orientated in the direction of the flow and their *b*-axis (intermediate axis) being imbricated. The subsurface architecture of a bed is thought to influence sediment–water interface exchange mechanisms, in particular the exchanges of soluble and fine particulate pollutants between the overlying river flow and the pore water (e.g. Salehin *et al.*, 2004; Packman *et al.*, 2007).

A number of studies have used idealized gravel bed configurations to isolate the effects of different deposit surface configurations (e.g. Dittrich and Koll, 1997; Lawless and Robert, 2001; Ferro, 2003; Sambrook Smith and Nicholas, 2005; Schmeekle *et al.*, 2007), but few have developed techniques to recreate bed conditions found in natural gravel-bed rivers. Recently, Buffin-Bélanger *et al.* (2003) developed a casting procedure which accurately reproduces the complexity of gravel-bed surfaces. Moulds were taken of a section of a gravel-bed in the field from which casts were produced and placed in the flume. It is clear that this will create a surface with the geometric structure of a natural gravel-bed, but it is impermeable and does not replicate subsurface vertical sorting. In addition, in narrow laboratory flumes, the size of the 'grains' on the cast are not well scaled with the width of the flume, possibly causing individual clasts to dominate the flow pattern within the flume width and to cause isolated roughness effects and enhanced flume sidewall effects.

A different approach to bed production was therefore studied here. Sediment beds were formed by feeding material into running water. The beds formed through sequential cycles of erosion and deposition and it is proposed that these beds currently offer a more appropriate way to simulate natural gravel-beds in laboratory flumes. The bed surface topography was measured in detail over these fed beds and compared to that of a screeded bed. In addition, measurements were made of bulk porosity and hydraulic conductivity, and high-spatial resolution measurements of fluid velocity were taken in a horizontal plan above these beds to derive turbulence and spatial flow characteristics. The aim of the paper is not to describe how these fed beds formed, but rather to (1) demonstrate that the bed surface topographies and (2) subsurface properties of fed beds more faithfully represent the topographies found in natural gravel-bed rivers, and (3) to demonstrate the importance of creating water-worked fed beds for simulating near-bed flow dynamics in gravel-bed rivers.

Methodology

Experimental set-up

The tests were conducted in a 18·3 m long, 0·5 m wide laboratory flume, with a working length of 15 m, which could be tilted to a produce a range of flume slopes (Figure 1). All the bed and water surface measurements were made relative to a datum plane, defined by two parallel rails running along either side of the flume. The distances from this datum plane to the bed and the water surface were measured using vernier point depth gauges. The depth of the water was controlled by

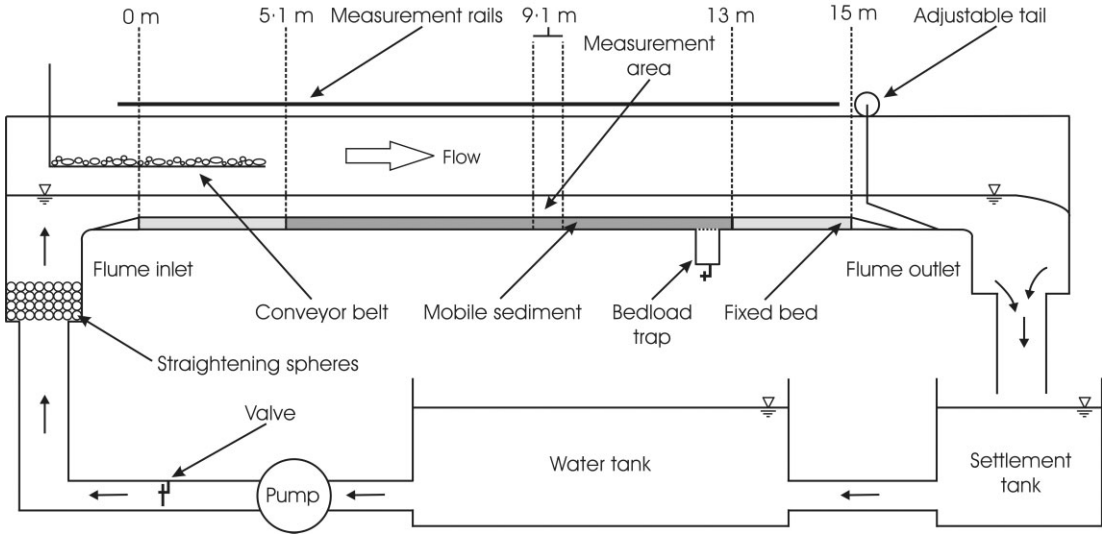

Figure 1. A schematic diagram of the laboratory flume layout.

DOI: 10.1002/esp

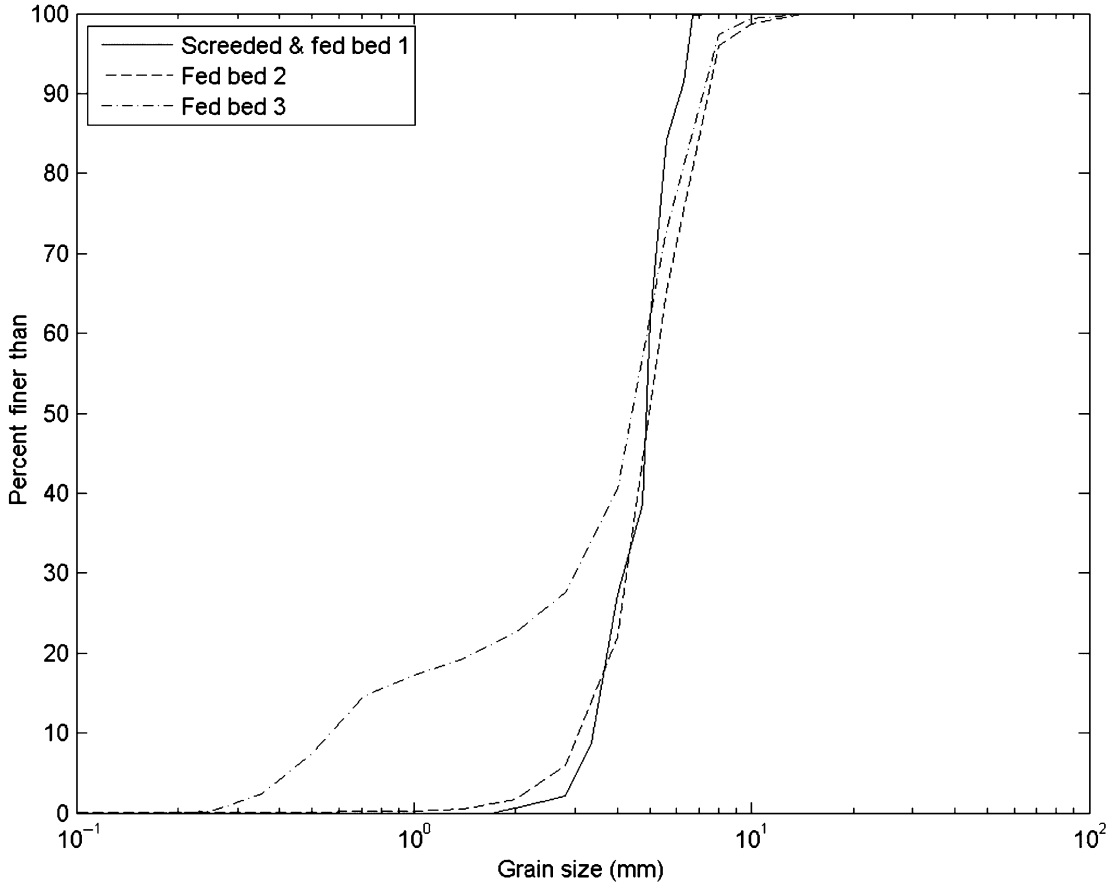

Figure 2. Grain-size distributions of the three mixtures used to create the four beds.

a sharp-edged adjustable weir at the downstream end of the flume. The flow rate was monitored using a pre-calibrated orifice plate in the upstream delivery pipe.

Three sediment mixtures were used to produce four different sediment deposits within the flume, one screeded and three fed beds. They were chosen to characterize the two predominant types of grain-size distributions observed in gravel-bed rivers: two mixtures had a log-normal, unimodal grain-size distribution and the third mixture had a slightly bimodal grain-size distribution (Figure 2). The former consisted of 100 per cent gravel quarried from alluvial deposits and was used to form a screeded bed and two fed beds (fed beds 1 and 2). The grains were not crushed and had the rounded properties of grains found in gravel-bed rivers. The bimodal mixture contained 75 per cent of the same gravel and 25 per cent sand obtained from the same deposits and was used to form the third bed (fed bed 3). Table I provides a summary of the parameters of the mixtures. The three mixtures were designed to produce similar values of D_{50}, the grain size at which 50 per cent of the bed material is finer, so that the scale of the grains in each of the beds was comparable. It is noted that the grain-size distributions are narrower than would be found in a gravel-bed river and precludes the finer material that would be found in the subsurface.

Table I. A summary of the parameters of the three mixtures used to form the four beds, where D_{50} and D_{84} are the grain sizes at which 50 and 84 per cent of the bed material is finer, respectively, $D_{\tilde{x}}$ is the mean grain-size, σ_D is the sorting coefficient, Sk_D is the skewness and Ku_D is the kurtosis of the volumetric grain-size distribution

Property	Screeded and fed bed 1	Fed bed 2	Fed bed 3
D_{50} (m)	0·00487	0·00497	0·00442
D_{84} (m)	0·00559	0·00700	0·00659
$D_{\tilde{x}}$ (m)	0·00468	0·00495	0·00380
σ_D (m)	0·00126	0·00140	0·00190
Sk_D (m)	0·00124	0·00107	0·00123
Ku_D (m)	0·00107	0·00109	0·00117

Bed formation

The method of bed formation chosen was based on the concept developed to form beds in laboratory flumes in order to study downstream fining (Paola *et al.*, 1992; Seal *et al.*, 1997; Toro-Escobar *et al.*, 2000), whereby sediment is fed into a running flume to form a sediment deposit. A conveyor belt was used to inject gravel into the flow at twice its transport capacity in order to form a deposit. The transport capacity was estimated from the Meyer-Peter and Müller (1948) equation for bedload transport discharge. Feed rates of 0·0624 kg m^{-1}, 0·0922 kg m^{-1} and 0·152 kg m^{-1} were used to form fed beds 1, 2 and 3, respectively. A channel slope of 0·0055 and a constant discharge of 0·0295 m^3 s^{-1} were selected for the formation of all three fed beds so that the time-scale was long enough to allow a progressive formation of the bed, but short enough for the bed to form within a reasonable time. The downstream adjustable weir was laid flat to the flume floor to allow the flow depth to adjust naturally to the changing bed conditions. The conveyor belt was mounted so that the sediment fell from the belt at approximately 200 mm above the fixed bed, with its downstream edge being 0·5 m upstream of the fixed bed (see Figure 1). The fixed bed was 60 mm higher then the steel flume floor. This resulted in the sediment descending, saltating and rolling over the fixed bed before falling onto the flume

DOI: 10.1002/esp

floor. It was found that no grains were completely transported out of the flume upon entry to the steel floor, and indeed came to rest very quickly upon impact with the floor.

Feeding was halted when the bed slope remained steady over a period of three hours. This was defined as occurring when the bed slope of the deposit was within 5 per cent of the bed slope measured for the previous measurement period. Since the bed slope was measured every 30 minutes this meant ensuring that this condition was met for six measurements of bed slope. A steady value of bed slope was taken to indicate conditions of equilibrium, where feed rate was equal to bedload transport rate.

For all three fed beds, the grains were observed to be transported and deposited in the manner of conventional bedload transport, resulting in the grains finding the most sheltered local position, and creating a configuration of imbricated grains. At the end of each day of feeding, the surface of the deposit displayed particle clusters and preferential orientation of the *a*-axis of the grains in the direction of the flow. This surface was then later covered after further feeding. It means that the layers within the deposit were all water-worked. The deposit would increase in depth through this process of feeding, transport and deposition, meaning that throughout the depth of the deposit the grains would be imbricated and represent all grain sizes present in the feed material. This created vertically sorted deposits through natural processes of transport and deposition. The resulting deposits adopted a bed slope of 0·00288, 0·00225 and 0·00224 for fed beds 1, 2 and 3, respectively, which are remarkably similar, reflecting the repeatability of the bed production approach. These slopes were measured relative to the flume slope. The screeded bed was formed by placing randomly mixed sediment into the base of the flume. This was not compacted and was screeded to a depth of 60 mm, such that the bed slope was equal to that of the channel.

Bed surface topography measurements

The final bed surface topography of the deposits was characterized by an orthogonal grid of bed surface elevation measurements. The elevation of each point was measured using a Keyence LC-2450 laser displacement sensor. This was moved over the bed surface in a pre-determined grid of measurement points by an automated positioning system located on the flume rails. The laser displacement sensor could measure to a resolution of 0·5 μm in the vertical, with each measurement being integrated over an area of 20×45 μm. The worst data set contained 0·8 per cent out of range readings, while it was typically 0·4 per cent. Given the low percentage of outliers, these errors can be assumed not to have altered significantly the results drawn from the topography measurements. Since the sensor was located on the positioning system on the flume rails, the sensor was not parallel to the bed surface of the fed beds. The data were therefore detrended in the streamwise and lateral directions using a simple linear interpolation to remove any spatial bias arising from this non-parallelism. The lateral slope was negligible for each bed and a bi-directional detrending was applied for completeness rather than because there was a large lateral bed slope to be removed from the data. The mean elevation was found and set to zero so that all elevations were given relative to the zero mean elevation of the bed surface.

Bed surface topography was measured over an area of 200×200 mm for the screeded bed and fed bed 1, and over an 250×250 mm area for fed beds 2 and 3. Each was performed at a spacing of 1 mm in both the streamwise and lateral directions. The measurement area was centred on the flume centreline. This was positioned to measure the bed surface topography over which the fluid velocity measurements were subsequently taken, so that the measurement positions of the velocity vectors and the bed surface elevations exactly corresponded. The resolution of the sensor and the measurement grid enabled the description of the features of the bed surface arrangement at a grain scale.

Subsurface measurements

The bulk porosity ϕ of the subsurface of the final bed deposits of fed beds 2 and 3 was measured and compared with those by Aberle (2007) from a screeded bed. Within the subsurface of the deposit, ϕ is equal to the ratio of the volume occupied by fluid V_f to the total volume V_0. The bulk porosity of the subsurface of the final bed deposits of fed beds 2 and 3 was therefore determined by measuring the volume of water V_f required to reach a water level equal to that of the minimum surface bed elevation. This volume was measured by adding known volumes of water into the flume. Before each measurement the flume was set to a negative slope so that the bed surface slope was horizontal. The flume was sealed at the upstream and downstream ends of the mobile section of bed. This provided a sealed section of bed of a length L of 7·8 m (0·1 m shorter than the total mobile section because of the sealing procedure). With knowledge of the mean stable water level relative to the flume floor d_f, V_0 can be calculated from wLd_f, where w is the width of the flume. For each deposit, these measurements were repeated three times to determine ϕ. Before each measurement the deposit was thoroughly drained and air dried.

Once these experiments were finished, an additional set of tests were carried out to estimate the hydraulic conductivity K of fed beds 2 and 3. Darcy showed experimentally, which has since been proved theoretically from simplifications made to the Navier-Stokes equations, that a simple relationship relates the instantaneous discharge through a porous medium to the local hydraulic gradient and the hydraulic conductivity at that point. In terms of the flow through the bed, it follows that

$$Q_b = -KA_b \frac{d_f}{\delta_b} \quad (1)$$

where Q_b is the instantaneous discharge through the bed, A_b is the cross-sectional area of the bed, and δ_b is the thickness of the bed, from which K can be derived. Hydraulic head is assumed to be approximated by d_f, and this is valid when the flow is considered to be steady. This assumption is valid for the conditions investigated because there were only very small changes in d_f over time because of the large volume of sediment for the water to drain through, and the values of Q_b were small. Darcy's law assumes that K over the area of the bed is homogeneous. If the flow through a large section of the bed is considered, the heterogeneity in the bed structure is essentially taken into account, producing an estimate of the average conductivity of flow through the bed.

The flume was again set to a negative slope so that the bed slope was zero, and the mobile bed section was sealed. The mobile section of the bed was steadily filled with water until the bed was totally saturated and the water was at a small depth above the bed surface. The bed level was measured at 0·1 m intervals along the length of the section using a point gauge, and were made relative to the channel floor. A mean value of δ_b was then derived. The cross-sectional area of the bed was given by summating the areas of the bed over the 0·1 m sections. A bedload slot trap was located 0·2 m from the downstream end of the sealed section of bed. It consisted of a rectangular opening in the base of the flume, a water-tight

DOI: 10.1002/esp

valve and rectangular collection boxes. The opening was covered with a fine mesh so that no grains could fall into the trap, and so that it was fully covered by the sediment during the bed formation. The flow through the bed was measured by opening the valve on the trap a small amount and continuously sampling the mass of water that had been discharged. The change in d_f during this discharge was measured by coring a small hole in the bed down to the channel floor, at a distance of 6·2 m from the trap, and measuring the water level within this hole using a point gauge. This distance from the trap was considered sufficient for the effects of the hole on the discharge out of the trap to be assumed negligible. The mass of water and d_f was measured every two minutes until a negligible mass of water (<0·3 kg) was collected during several two-minute periods. For each deposit this was carried out three times, with deposits again being thoroughly drained and air dried before each measurement.

Velocity measurements

A two-dimensional Dantec Particle Image Velocimetry (PIV) system was used to provide detailed spatial measurements of fluid velocity over the two beds. It was operated at 9 Hz, and this allowed five and a half minutes of the flow to be sampled. Previous approaches to utilize PIV to study the hydrodynamics of flows over rough sediment boundaries have taken measurements at one lateral position across the bed by using a vertical light sheet orientated normal to the bed surface (in a vertical plane), in order to obtain streamwise and vertical velocities (e.g. Tait *et al.*, 1996; Campbell *et al.*, 2005; Sambrook Smith and Nicholas, 2005). A different approach was adopted here, whereby the light sheet was located parallel to the bed surface to obtain streamwise and lateral velocities over a larger section of the bed, but at one vertical height above the bed. This allowed velocity measurements at many more measurement locations over the bed than is possible with the use of PIV in a vertical plane. In addition, it enables the characterization of the areal variability in streamwise velocities, which is not possible with vertical plane PIV measurements. A glass plate was very lightly positioned on the water surface to ensure there were no reflections from the rippled water surface. The light-sheet was positioned at 10 mm above the maximum bed elevation of the bed, and the cameras imaged a measurement area of 198·4 × 200·0 mm^2 at 9·1 m from the inlet (see Figure 1). An interrogation area of 32 × 32 pixels was used in the cross-correlation of the images. The interrogation areas were overlapped by 50 per cent in both the streamwise and lateral direction to increase the probability that particles near the edges of an interrogation area contributed to the velocity calculation. This provided 62 velocity measurements in each lateral direction and 61 measurements in each streamwise direction, and resulted in 3782 measurement locations within the image area. There was a separation distance of 3·15 mm between each velocity vector measurement (in both the streamwise and lateral direction). The spatial resolution of the velocity measurements is equal to the length of the interrogation area. This gives a spatial resolution of 6·30 mm, and allows the flow field to be measured at the grain-scale. This means that the PIV measurements were able to resolve large-scale structural features rather than those with dimensions of the Taylor's microscale, which is generally the case in PIV (Dantec, 2000). Further details on the PIV set-up and image processing routines can be found in Cooper (2006) and Cooper and Tait (2008).

The PIV measurements were performed at similar levels of relative submergence d/k for each of the four beds (Table II),

Table II. A summary of the experimental conditions, where S is the bed slope (equal to a summation of the flume slope and the slope of the deposit), Q is the flow discharge, d is the flow depth, k is the range of bed surface elevations, u_* is the bed shear velocity (calculated from the depth-slope product), and Re is the flow Reynolds number

Bed	S	Q (m^3 s^{-1})	d (m)	d/k	u_* (m s^{-1})	Re
Screeded	0·00600	0·0408	0·0900	5·51	0·0627	62 132
Fed Bed 1	0·00288	0·0295	0·0900	5·66	0·0432	44 957
Fed Bed 2	0·00285	0·0280	0·0900	5·93	0·0430	42 618
Fed Bed 3	0·00284	0·0245	0·0845	6·16	0·0419	37 388

where d is the flow depth and where k is the range of bed surface elevations. This allowed the effect of bed surface topography, from the four beds, to be isolated from the effects of differences in relative submergence. The flow conditions were below those required for bed movement, so that the beds were static. For each experimental run, a steady flowrate was introduced and the downstream weir adjusted to achieve uniform depth within the measurement area and for as large a reach as possible.

For each experimental run, the instantaneous velocities u_i were used to derive turbulence and spatial flow characteristics. This was achieved by time-averaging these velocities and applying a Reynolds decomposition. This was supplemented with spatial averaging and a spatial decomposition. The tensor notation, with the Einstein convention, means that u_i (i = 1, 2, 3) corresponds to the velocity components u, v and w. The Reynolds decomposition involved taking the velocity field and decomposing it into time-averaged $\bar{u}_i$ and temporally fluctuating components u_i', such that $u_i = \bar{u}_i + u_i'$. The spatial variability in the time-averaged flow field that occurs over water-worked gravel-beds (Cooper, 2006; Cooper and Tait, 2008) can be taken into account explicitly only by supplementing the time-averaging with spatial area averaging in the plane parallel to the averaged bed surface. The averaging procedure for spatial area averaging at level z is defined as (Nikora *et al.*, 2001)

$$\langle V \rangle(x,y,z,t) = \frac{1}{A_f} \int_{A_f} \int V(x',y',z,t) \mathrm{d}x' \mathrm{d}y' \qquad (2)$$

where V is the flow velocity defined in the fluid to be spatially-averaged over the fluid domain A_f. This fluid domain is assumed to be planar and parallel to the averaged bed surface, and to be the area occupied by the fluid on the x, y-plane at level z within the total area A_0. The use of the terms x' and y' are used to make it clear that the dependence of $\langle V \rangle$ on (x, y) is due solely to the variation in A_f with (x, y). The averaging area A_0 is often taken to be a thin streamwise slab in order to preserve the characteristic spatial variability in the flow in the vertical direction. Therefore the PIV measurements are appropriate for applying spatial averaging, and in this case $A_0 = A_f$. This was combined with a decomposition of time-averaged variables into spatially averaged (denoted by angle brackets) and spatially fluctuating (denoted by a wavy overbar) components, that is analogous to the Reynolds decomposition for instantaneous variables, such that $\bar{u}_i = \langle \bar{u}_i \rangle + \tilde{u}_i$. The spatial fluctuations arise from the difference between the double-averaged $\langle \bar{u}_i \rangle$ and time-averaged $\bar{u}_i$ values ($\tilde{u}_i = \bar{u}_i - \langle \bar{u}_i \rangle$, $\langle \tilde{u}_i \rangle = 0$) similar to the conventional Reynolds decomposition of $u_i' = u_i - \bar{u}_i$. In this way, by combining time- and spatial-averaging approaches, it was possible to derive the double-averaged characteristics of the flow, such that both the temporal and spatial variability in the flow is explicitly taken into account. These characteristics over the three fed beds were compared with a screeded bed.

DOI: 10.1002/esp

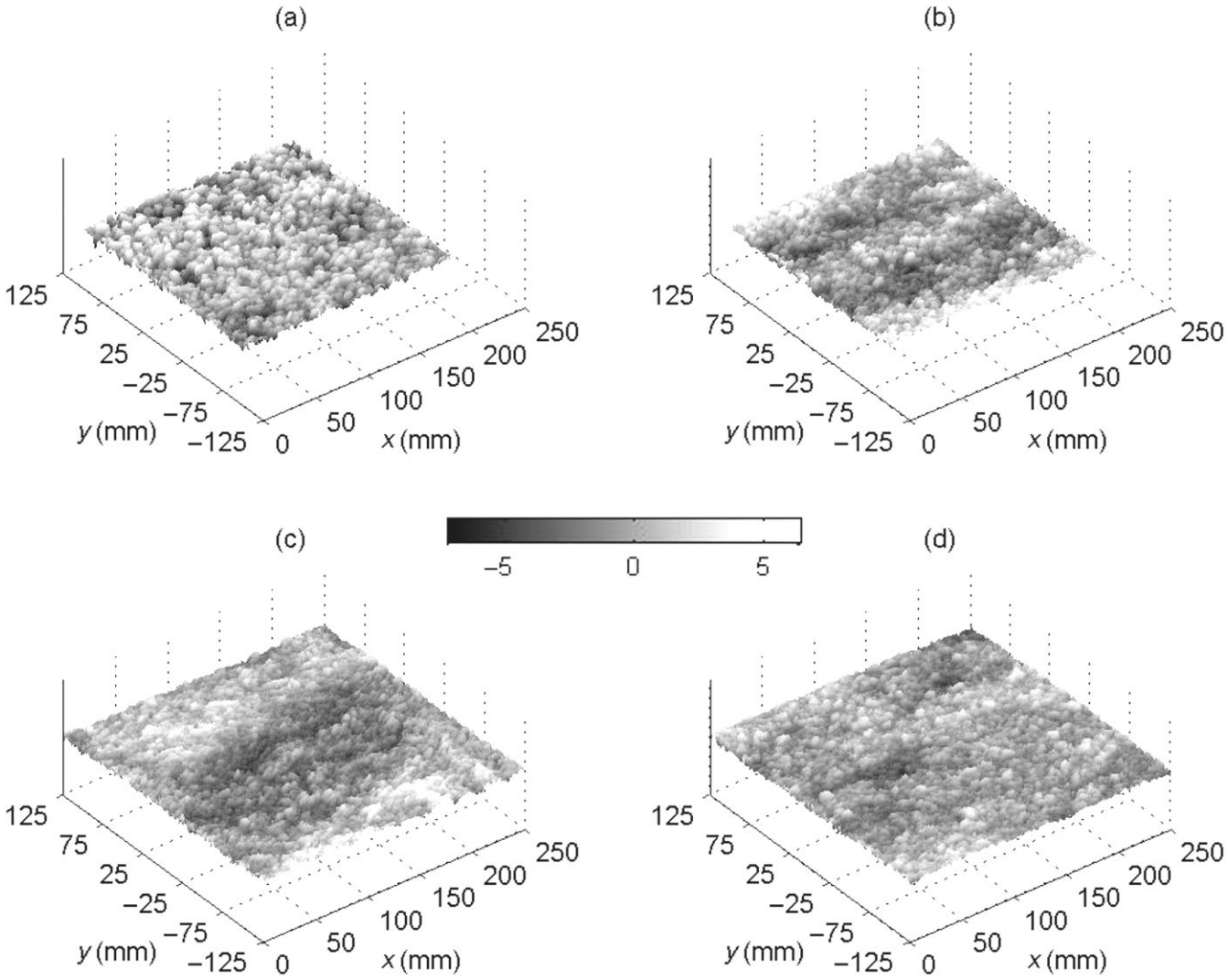

Figure 3. Digital elevation models of the bed surface topography for (a) the screeded bed; (b) fed bed 1; (c) fed bed 2; and (d) fed bed 3. The greyscale relates to the departure in elevation from the zero mean surface elevation (mm). A lateral position y of 0 mm denotes the centreline of the flume and the increasing values in the streamwise position x are in the direction of the flow.

Results and Discussion

Bed surface properties

Digital elevation models

The surface texture of the three fed beds and the screeded bed can be visualized by representing the bed elevations from the zero mean surface elevation z_b as a Digital Elevation Model (DEM) (Figure 3). It shows that the surface topography of the screeded bed is irregular with random grain-scale protrusions around the mean bed elevation. It has a fairly flat uniform surface and the pore space between individual grains is clearly visible, providing an impression of a loose surface (Figure 3a).

In contrast, fed bed 1, which is created from the same bed mixture, is well imbricated, with smaller pore spaces and it is well-packed (Figure 3b). It also has a more organized pattern. There are clear longitudinal zones of higher elevations which alternate with longitudinal zones of lower elevations. This suggests the presence of alternating longitudinal troughs and ridges, which are often a feature of water-worked gravel beds (Nezu and Nakagawa, 1993; Tait, 1993; Shvidchenko and Pender, 2001). This is in accordance to what could be seen along the whole deposit. Apart from these features the bed was relatively flat (at the macroscopic scale) and had a uniform bed slope along the whole length of the deposit, and displayed no larger scale structuring. However, there was evidence of an abundance of particle clusters along the whole length of the deposit, which are commonly associated with water-worked gravel beds.

Fed bed 2 is equally well packed and imbricated, and, like the unimodal bed, has alternating zones of higher and lower elevations (Figure 3c). There is a zone of higher elevations towards the top right of the plot, followed by a larger zone of lower elevations which is diagonally orientated. There is then a small area of lower elevations located in the bottom right of the plot where a depressed diagonal zone is evident from the bottom left to the mid-right of the image. This suggests the presence of a larger longitudinal trough than was seen for fed bed 1, flanked by two ridges to the top and bottom. This is again in accordance to what could be seen along the whole deposit, which was macroscopically flat and covered in particle clusters.

The third fed bed, unlike fed beds 1 and 2, has no clear surface structuring (Figure 3d). There are only local depressions and local areas of higher elevation, which do not appear to be part of any organized pattern, but the grains are well packed and imbricated. This bed also displayed an abundance of particle clusters on a flat (at the macroscopic scale) surface. The important feature is that the surface textures of the three

DOI: 10.1002/esp

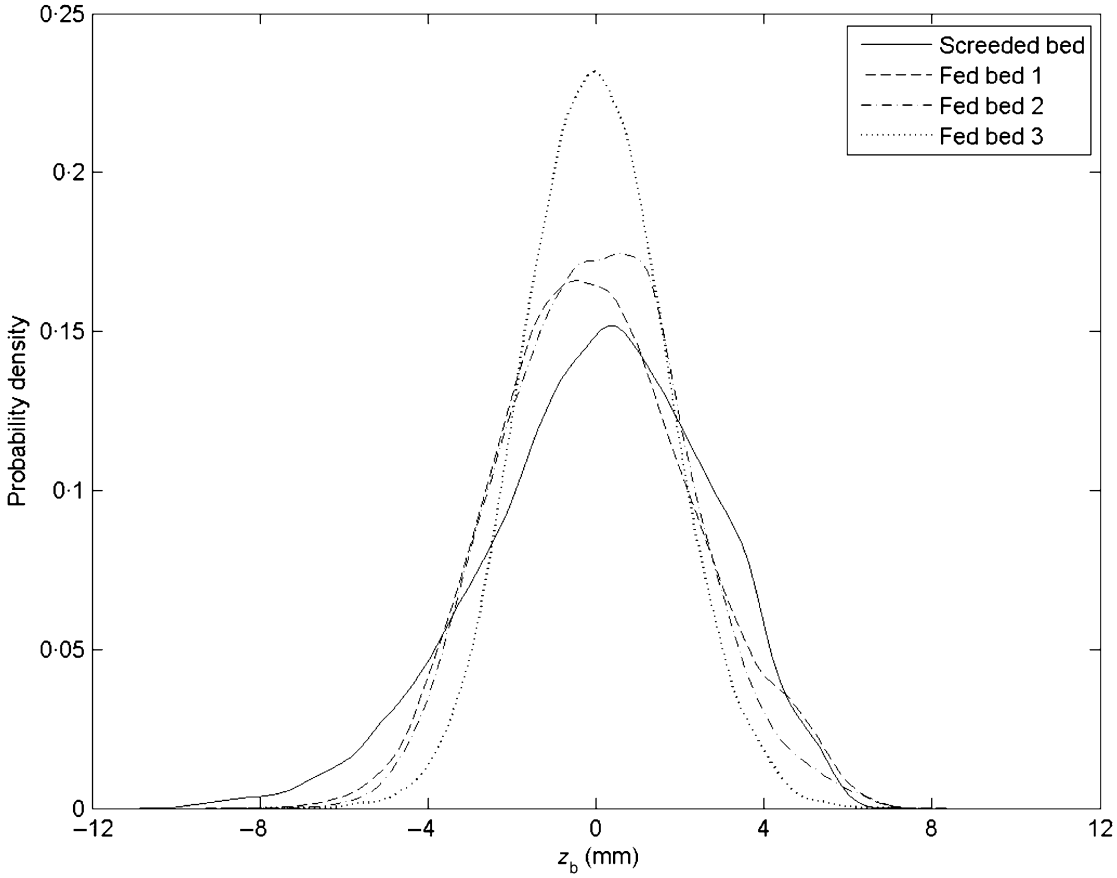

Figure 4. The probability density function of the bed elevations from the zero mean surface elevation z_b for the four beds.

fed beds are distinctly different from the screeded bed, but feeding still produces relatively flat (at the macroscopic scale) deposits that are suitable for achieving uniform flow within the flume.

Probability density functions

The probability density functions (PDFs) of z_b reveal differences between each of the four beds (Figure 4). The PDFs for fed beds 1 and 2 show the greatest similarity in shape, and this reflects that both were created in the same manner from similar gravel mixtures. This is despite the screeded bed and fed-bed 1 being created from exactly the same mixture. The screeded bed has a slightly negatively skewed distribution of z_b, but the distributions for the three fed beds are very slightly positively skewed (Table III). This supports the conclusion of Nikora *et al.* (1998) that manually created beds are negatively skewed and that natural beds are positively skewed. Positive skewness is said to indicate the existence of a water-worked surface and of an armouring effect on the bed (Brown and Willetts, 1997; Nikora *et al.*, 1998; Marion *et al.*, 2003; Smart *et al.*, 2004; Aberle and Nikora, 2006). The positive skewness is slightly higher for fed beds 1 and 2 created purely from gravel, reflecting the more structured surface seen in the DEMs.

The range of bed surface elevations k is a measure of geometrical roughness and Table III shows that k is smaller over the fed beds, perhaps owing to the greater particle imbrication seen in the DEMs. It is especially low for fed bed 3 which is likely to be due to the infilling of the interstices between the gravel particles by the sand within the mixture. This difference in k is also reflected in the standard deviation in bed surface elevations σ_b (Table III). It has been argued that σ_b can be interpreted as a characteristic vertical roughness length of water-worked gravel beds (Nikora *et al.*, 1998; Aberle and Smart, 2003; Aberle and Nikora, 2006). It shows that this roughness length is lower over the three fed beds, especially so over the fed bed 3, reflecting the differences in the DEMs of the four beds.

Table III. A summary of the bed surface properties of the three beds, where σ_b is the standard deviation, k is the range, Sk_b is the skewness and Ku_b is the kurtosis of the distribution of bed surface elevations z_b, respectively, l_{x_0} and l_{y_0} are the correlation lengths of z_b in the streamwise and lateral directions, respectively, and H_x and H_y are the Hurst exponents for the streamwise and lateral variations in z_b, respectively

Property	Screeded	Fed bed 1	Fed bed 2	Fed bed 3
σ_b (m)	0·00266	0·00233	0·00214	0·00170
Sk_b	–0·397	0·169	0·0985	0·0462
Ku_b	2·991	2·755	2·837	3·015
k (m)	0·0163	0·0159	0·0152	0·0137
l_{x_0} (m)	0·00576	0·00969	0·0135	0·00764
l_{y_0} (m)	0·00523	0·0112	0·0149	0·00778
H_x (m)	0·472	0·465	0·452	0·463
H_y (m)	0·371	0·355	0·320	0·368

Second-order structure functions

Although the PDFs show evidence of differences in the bed surface between the four beds, they fail to clearly describe the degree of surface particle organization. This can be assessed by using a two-dimensional second-order structure function of the bed surface elevations, as used by Goring *et al.* (1999). The structure function $D_b(l_x,l_y)$ of bed surface elevation $z_b(x,y)$ is defined as

DOI: 10.1002/esp

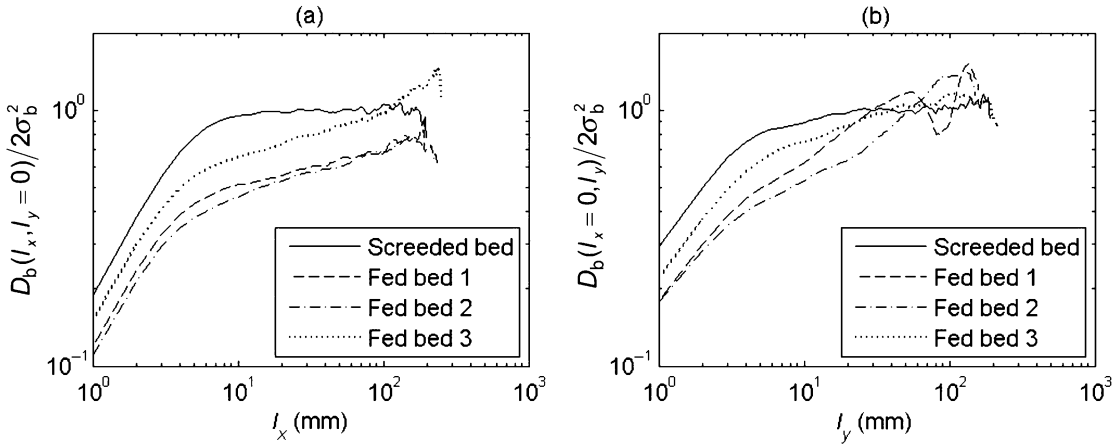

Figure 5. Second-order structure functions D_b of the bed surface elevations normalized by $2\sigma_b^2$ for (a) $l_y = 0$ and (b) $l_x = 0$.

$$D_b(l_x, l_y) = \frac{1}{(N_b - n_b)(M_b - m_b)} \sum_{i=1}^{N_b - n_b} \sum_{j=2}^{M_b - m_b} \left\{ z_b(x_i + n_b \delta x, y_j + m_b \delta y) - z(x_i, y_j) \right\}^2 \quad (3)$$

where $l_x = n_b \delta x$, and $l_y = m_b \delta y$ are spatial lags, n_b and m_b are multiplying coefficients, δx and δy are the sampling intervals, and N_b and M_b are the total number of measured bed elevations, in the streamwise x and lateral y directions, respectively. For a globally homogeneous random field, the second-order structure function has the following relationship with the correlation function $R_b(l_x, l_y)$

$$D_b(l_x, l_y) = 2[\sigma_b^2 - R_b(l_x, l_y)] \quad (4)$$

This shows that at large spatial lags when $R_b(l_x, l_y) \to 0$ and $D_b \to 2\sigma_b^2$ the data are spatially uncorrelated and the lags at which $D_b \to 2\sigma_b^2$ can be used to derive characteristic streamwise and lateral length scales (Nikora *et al.*, 1998).

Figure 5 shows the second-order structure functions for the four beds, which is plotted in terms of $D_b(l_x, l_y)/2\sigma_b^2$. It is reasonable to compare the four beds directly given the similarity in the D_{50} of the beds (Table I). Figure 5a shows the variation in $D_b(l_x, l_y = 0)/2\sigma_b^2$ with l_x and Figure 5b shows the variation in $D_b(l_x = 0, l_y)/2\sigma_b^2$ with l_y. Low values of $D_b(l_x, l_y)/2\sigma_b^2$ indicate high levels of correlation with l_x and l_y, such that at a value of zero a perfect correlation exists. As $D_b(l_x, l_y)/2\sigma_b^2$ increases to unity, the degree of correlation decreases. At unity, the bed elevations have no correlation and the bed surface topography can be sensibly considered random in organization.

It is believed that all second-order structure functions for water-worked beds can be subdivided into scaling, transition and saturation regions (Nikora *et al.*, 1998; Nikora and Walsh, 2004). Given that the second-order structure functions in Figure 5 follow the pattern that has been observed by others (Robert, 1988, 1991; Nikora *et al.*, 1998; Butler *et al.*, 2001; Nikora and Walsh, 2004; Aberle and Nikora, 2006), such a subdivision can be applied. At small spatial lags, the structure functions can be approximated by the power function $D_b(l_x, l_y = 0)/2\sigma_b^2 \propto l_x^{2H_x}$ and $D_b(l_x = 0, l_y)/2\sigma_b^2 \propto l_y^{2H_y}$ (Nikora *et al.*, 1998), and this corresponds to the scaling region. The scaling exponent H is known as the Hurst exponent. At sufficiently large lags $D_b(l_x, l_y)/2\sigma_b^2 = 1$ and this is the saturation region. Only one of these functions does not reach this region. Between these two regions, the structure functions are curved and are within the transition zone (Nikora *et al.*, 1998; Nikora and Walsh, 2004).

Figure 5 reveals that for $D_b(l_x, l_y = 0)/2\sigma_b^2$ and $D_b(l_x = 0, l_y)/2\sigma_b^2$ the extent of the scaling region is up to $l_x, l_y \approx 3$–4 mm which is very similar for each of the four beds, and given that it is the same in the streamwise and lateral direction it suggests that the surface structure is similar at small lags, but the transition zones are longer over the fed beds. This may indicate that over these beds there are bed features that are larger than the grain scale, given that the scaling region exists only up to $l_x, l_y \approx 3$–4 mm. However, the very short transition zone for the screeded bed may indicate that this bed is unlikely to have this scale of bed structure. A comparison of $D_b(l_x, l_y = 0)/2\sigma_b^2$ and $D_b(l_x = 0, l_y)/2\sigma_b^2$ shows that for a given bed the shapes of the curves are similar, although the curves are separated by a small vertical offset ($D_b(l_x = 0, l_y)/2\sigma_b^2 > D_b(l_x, l_y = 0)/2\sigma_b^2$. The vertical offset is consistent with the difference in second-order structure functions in these two directions (Aberle and Nikora, 2006). This is due to a lower degree of coherency in the bed surface elevations in the lateral direction.

The difference in the spatial lags at which $D_b(l_x, l_y)/2\sigma_b^2 \to 1$, the lower limit of the saturation region, reflects the difference in the correlation lengths of the bed surface elevations. The streamwise correlation length l_{x_0} and the lateral correlation length l_{y_0} can be estimated from the curves in Figure 5 following the method outlined in Nikora *et al.* (1998). These values are given in Table III and show that there is a considerable difference between the screeded and fed beds. The fed beds have longer correlation lengths in both the streamwise and lateral direction, supporting the suggestion that these beds have larger scale bed features. The lengths are higher over fed beds 1 and 2, which reflects the greater structure in the bed surface elevations. Nikora *et al.* (1998) found that, on average, the vertical correlation length scale σ_b is less than half the horizontal roughness length scales for natural gravel-bed rivers. Table III shows that this condition only holds for the three fed beds, with σ_b being approximately half the horizontal scales for the screeded bed. This suggests that the roughness scales of the three fed beds more faithfully represent those of natural gravel-bed rivers.

The scaling (or Hurst) exponents H_x and H_y are estimated from within the scaling region. These estimates are shown in Table III and show that they are higher over the screeded bed than the fed beds. The value of the Hurst exponent is inversely proportional to the degree of complexity in the surface topography (Bergeron, 1996). As such, the exponents again reveal that the screeded bed has a less complex topography then the fed beds. The H_x values range from 0·45 to 0·47, which is smaller than has been reported before (Nikora *et al.*, 1998; Butler *et al.*,

DOI: 10.1002/esp

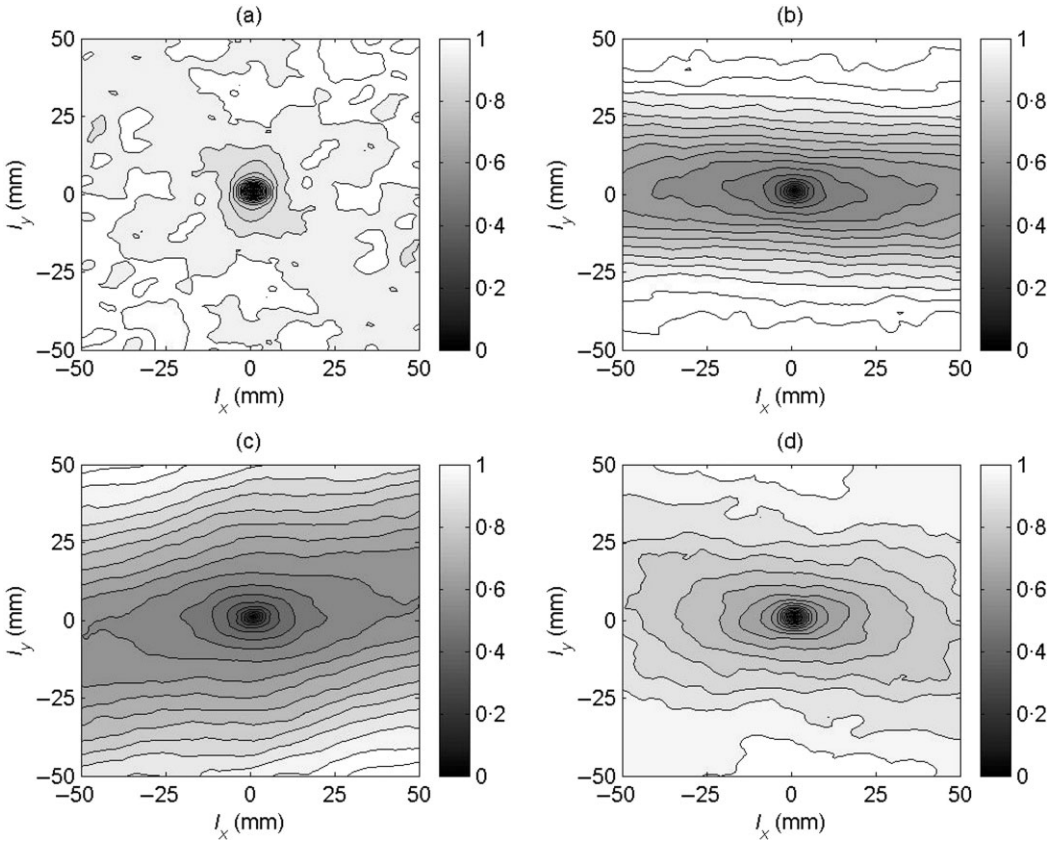

Figure 6. Contour plots of the second-order structure functions D_b of the bed surface elevations normalized by $2\sigma_b^2$ for (a) the screeded bed; (b) fed bed 1; (c) fed bed 2; and (d) fed bed 3.

2001; Nikora and Walsh, 2004; Aberle and Nikora, 2006) owing to the smaller grain sizes on the bed surface (Robert, 1988; Bergeron, 1996; Aberle and Nikora, 2006).

Observations suggest that individual particles and particle imbrications on the surface of an armoured gravel bed have preferential alignments, with their *a*-axis parallel to the flow direction, their *b*-axis perpendicular to the flow direction, and their *c*-axis (short axis) orthogonal to the flow direction (Allen, 1982; Marion *et al.*, 2003; Aberle and Nikora, 2006). Such a prevailing arrangement of the bed surface should reveal itself in the contour plots of $D_b(l_x,l_y)/2\sigma_b^2$, shown in Figure 6. Maximum spatial lags of ±50 mm in both the streamwise and lateral direction have been chosen because these are much larger than the maximum grain size of 14 mm. The contour lines for the two-dimensional structure function for the screeded bed are largely circular, suggesting that the particles are not oriented in any prevalent direction. This indicates an isotropy in this surface structure and a random organization. The correlation between z_b and l_x,l_y rapidly falls with increasing spatial lags, such that there are areas of separately formed circular patterns which are up to the size of the maximum grain size in the bed mixture. This could represent depressions between large particles (Nikora and Walsh, 2004), which reflects the less imbricated surface depicted in its DEM.

However, the contour lines for the two-dimensional structure function for the fed beds are characterized by an elliptical shape, reflecting an anisotropic surface structure. This shape is observed at scales larger than the grain-scale, and there is a similarity in the gradient of change in $D_b/2\sigma_b^2$ with l_x,l_y over both this scale and the grain-scale. This indicates that the elliptical shape is due to a combination of the effects of individual particle alignments and imbrications (micro-bedforms). The major axes of the elliptical contours are aligned in the direction of the flow (aligned with increasing l_x) indicating that the majority of the particles and their imbrications rest with their *a*-axis along the flow. The minor axis of the contour lines is aligned with the prevailing orientation of their *b*-axis, which is perpendicular to the flow. This suggests that the fed beds exhibit evidence of surface armouring. The elliptical form is more prominent over fed beds 1 and 2, demonstrating that these two beds exhibit stronger evidence of armouring. The fed beds have strong streamwise coherency at small lateral lags. This indicates the presence of longitudinal grain-scale structures, as seen in the DEMs of the beds. This streamwise correlation extends well beyond the streamwise size of the plot which indicates that these structures are long in their streamwise extent. These structures do not appear to have a single dominant lag in the lateral direction and the lateral correlation becomes negligible at small lateral lags, indicating that the longitudinal structures are relatively narrow in their lateral extent. The values of $D_b(l_x,l_y)/2\sigma_b^2$ reduce more quickly in the lateral direction for fed bed 1, which shows that the longitudinal structures are narrower, as seen in the DEMs.

Subsurface bed properties

The fed beds were formed through sequential cycles of erosion and deposition which meant that they exhibited a different subsurface structure to that of the screeded bed. The side view photographs of the deposits revealed that for the screeded bed, as expected, there was no preferential arrangement or structuring of the grains, with little interlocking. Whereas for the fed beds, the angle of the grains in the subsurface reflected the angle of those found on the surface. On average, the *a*-axis of the grains was in the direction of the flow at an angle of ~30–40° to the flume floor. There was also greater

DOI: 10.1002/esp

particle imbrication, particularly at this angle, and the grains were more tightly packed. Fed bed 3 also had thin layers of sand that extended in the streamwise direction along the whole length of the deposit.

The bulk porosities for fed bed 2 are 17·8 per cent, 17·2 per cent and 17·4 per cent from the three measurements, and 11·7 per cent, 12·3 per cent and 12·1 per cent for fed bed 3. This demonstrates the reproducibility of the experimental technique used to measure bulk porosity. The values are significantly lower than the average value of 23·2 per cent measured by Aberle (2007) for a compacted screeded bed with a static armour. They are also lower than the value of bulk porosity assumed by many for gravel-bed deposits (Diplas and Sutherland, 1988; Lisle and Lewis, 1992; Marion and Fraccarollo, 1997). Nevertheless, they do fall well within the range of values measured by Milhous (2001) in several gravel-bed rivers. Fed bed 3, in particular, which was created from a gravel–sand mixture, has also almost exactly the same porosity as measured by Carling and Reader (1982) for a similar mixture. Since porosity is dependent on the grain-size distribution of the subsurface, the porosity values from the fed beds and Aberle's (2007) screeded bed can be compared directly only by scaling the values according to grain-size. Based on the median or mean grain diameter and using its relationship with porosity reported by Komura (1963) and Carling and Reader (1982), respectively, the measured porosity values for Aberle's bed can be scaled according to the median and mean grain diameter of fed beds 2 and 3. This gives porosity values of 24·0 per cent and 24·4 per cent based on Komura (1963), and values of 26·4 per cent and 28·0 per cent based on Carling and Reader (1982) for this bed. This clearly shows that the bulk porosity is lower for the fed beds. It is acknowledged that the use of the median or mean grain diameter for scaling cannot fully account for the differences in the width of the grain-size distributions between the fed beds and Aberle's.

To gain greater understanding of how the subsurface differs between the beds, the hydraulic conductivity of fed beds 2 and 3 was quantified. The change in Q_b with d_f/δ_b is shown in Figure 7 for each of the three tests over the two beds, when the water level was less than the maximum bed elevation. The plots clearly show the repeatability of the tests, with the three tests over both of the beds producing very similar results. The flow through the bed pore follows Darcy's law, with the increase in Q_b with d_f/δ_b being approximately linear. A least-squares fit of the form of Equation 1 gives y-axis intercept values close to zero and R^2 values of 0·99 and 0·97 for fed beds 2 and 3, respectively. Therefore Darcy's law can be applied for estimating K. For fed bed 2 this gives $K = 1{\cdot}00 \times 10^1$ m s^{-1}, and a lower value of $K = 4{\cdot}07 \times 10^5$ m^{-1} for fed bed 3. This indicates that the conductivity is an order of magnitude lower within fed bed 3, and this might reflect the infilling of the interstices between the gravel particles by the sand during the formation of the bed, which occurred throughout the depth of the deposit. Based on the porosity of the subsurface and the D_{50} of the bed mixture, the Kozeny-Carman equation (Kozeny, 1927; Carman, 1937) for Aberle's (2007) compacted screeded bed gives a predicted K of 0·0149 m^{-1}. This is very close to the range of 1–0·01 m^{-1} that has been reported for unconsolidated gravel (Bear, 1972). These values are therefore also likely to apply for the screeded bed, indicating that the permeability is likely to be much higher within screeded beds than fed beds. It means that the screeded bed could have been classified as pervious, and the fed beds as semi-pervious (Bear, 1972). As a means of visualizing the difference, fed bed 2 has a conductivity

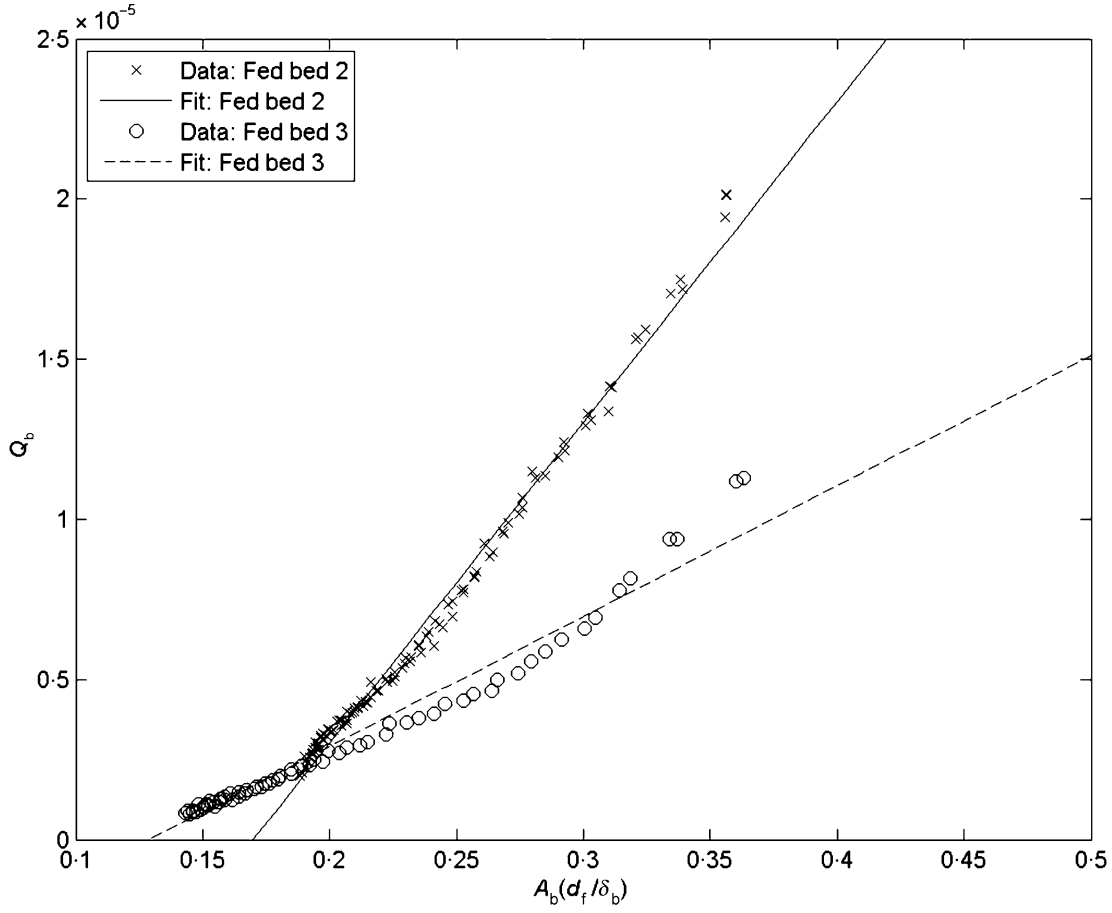

Figure 7. Variation in the instantaneous discharge through the bed Q_b with hydraulic gradient $A_b(d_f/\delta_b)$ for fed beds 2 and 3.

DOI: 10.1002/esp

value at the lower range reported for unconsolidated sand, or gravel and sand, and fed bed 3 lies at the transition between this and very fine sand, silt, loess or loam (Bear, 1972).

The bulk porosities and hydraulic conductivities of the two fed beds have a remarkable similarity to those measured in poorly sorted lithofacies (Heinz *et al.*, 2003; Barrash and Reboulet, 2004). The side-view photographs also revealed a preferential particle orientation and direction of imbrication which is consistent with that found in this lithofacies (Heinz *et al.*, 2003; Kostic *et al.*, 2005). Therefore, it can be concluded that the fed bed deposits strongly reflect the characteristics of this lithofacies, a facies that is common in gravel-bed deposits (e.g. Steel and Thompson, 1983; Smith, 1990; Siegenthaler and Huggenberger, 1993). The cyclic sediment feeding replicates the transport and depositional processes that are thought to produce these lithofacies, suggesting that fed beds are able to reproduce, in a simplified and basic manner, the subsurface properties of a given lithofacies. The properties described above for the screeded bed mean that, although screeded beds that have been water-worked for a period of time may contain surface properties akin to natural gravel beds, they will not recreate the subsurface properties of well-established gravel-bed river deposits. This has important consequences for studying sediment–water interface exchange mechanisms, such as the exchange of soluble and fine particulate pollutants between the overlying river flow and the pore water.

Near-bed flow properties

It has been shown that fed beds produce bed surface and subsurface properties that strongly resemble those found in gravel-bed rivers. However, it is important to investigate whether these geometrical differences significantly impact upon near-bed flow dynamics. The temporal and spatial characteristics of the flow over the screeded and fed beds are summarized in Table IV and scaled by bed shear velocity u_*. The streamwise turbulence intensity $\langle\sqrt{\overline{u'^2}}\rangle/u_*$ and the majority of the lateral turbulence intensity $\langle\sqrt{\overline{v'^2}}\rangle/u_*$ values are higher over the fed beds. This reveals that the level of turbulence within the flow is lower over the screeded bed. Results for the degree of spatial variability in the flow reveal different conclusions. The form-induced intensities $\sqrt{\langle\tilde{u}^2\rangle}/u_*$ and $\sqrt{\langle\tilde{v}^2\rangle}/u_*$ are simply the standard deviation in $\bar{u}$ and $\bar{v}$ over the bed scaled by u_*, and are a measure of the degree of spatial variability in $\bar{u}$ and $\bar{v}$, respectively. It can be seen that the fed beds experience similar degrees of spatial variability in $\bar{u}$, with the level of spatial variability being well scaled by u_*. On the other hand, the fed beds typically have higher levels of spatial variability in $\bar{v}$. The skewness values for the distribution of $\bar{u}$ over the bed $Sk_{\bar{u}}$ indicate that the distributions over all four beds are slightly negatively skewed, and express no significant difference in their levels of kurtosis $Ku_{\bar{u}}$. The only study that presents results of the skewness of the distributions of $\bar{u}$ is by Barison *et al.* (2003). Although they did not provide any skewness values, the distributions over an armouring gravel bed were also all found to be negatively skewed. The skewness values suggest that that the flow over the screeded and fed beds has localized areas of distinctly low $\bar{u}$ balanced by large areas of just slightly higher-than-average $\bar{u}$. The skewness $Sk_{\bar{v}}$ and kurtosis values $Ku_{\bar{v}}$ reveal that the distributions of $\bar{v}$ are all positively skewed and leptokurtic, but the degree of non-normality is less over the fed beds.

Table IV. A summary of the temporal and spatial characteristics of the near-bed flow field over the four beds

Property	Screeded	Fed bed 1	Fed bed 2	Fed bed 3
$\langle\sqrt{\overline{u'^2}}\rangle/u_*$	1·90	2·10	1·86	2·31
$\langle\sqrt{\overline{v'^2}}\rangle/u_*$	0·705	1·06	1·12	0·851
$\sqrt{\langle\tilde{u}^2\rangle}/u_*$	0·989	0·916	1·01	0·992
$Sk_{\bar{u}}$	–0·573	–0·0831	–0·991	–0·275
$Ku_{\bar{u}}$	2·82	1·67	3·49	3·10
$\sqrt{\langle\tilde{v}^2\rangle}/u_*$	0·176	0·141	0·207	0·215
$SK_{\bar{v}}$	3·34	0·0875	1·02	0·604
$Ku_{\bar{v}}$	41·1	18·6	24·0	25·7

These conclusions on the higher levels of turbulence intensity over the fed beds can be partly explained by the bed surface topography results explained above, particularly by the lower levels of bed surface roughness. But the differences between the screeded and fed beds could also possibly be partially explained by the differences in bulk porosity and how the void spaces are arranged. In the case of the screeded bed, the porosity is larger than for the fed beds and the void spaces are randomly organized within the subsurface. This is likely to induce greater exchange of fluid between the subsurface and the overlying flow than would be observed over the fed beds. For example, there is likely to be more incursion (or sweep) -like flow events from the overlying flow into the subsurface, and similarly, more ejection-like events transferring fluid from the bed to the overlying flow. The random organization of the bed surface topography and subsurface is not likely to concentrate the incursion- and ejection-like flow events in particular regions. Furthermore, it is not likely to produce a significant difference in the number of the two kinds of events occurring over the bed. This will clearly influence the near-bed flow structure and it will mean that there is a reduced level of spatially averaged turbulence intensity for two reasons: (i) at a given location over the bed, the temporal fluctuations, on a time-averaged basis, will tend towards zero as the sign of the fluctuations from the two flow types counteract each other; and (ii) over the whole bed, spatial averaging of the turbulence intensities at single locations over the bed will further reduce its magnitude due to the even spatial organization and relative number of the two flow events over the bed. In contrast, the fed beds have a reduced bulk porosity and exhibit preferential particle orientation and direction of imbrication in their subsurface. Therefore this is likely to cause a spatial heterogeneity in the distribution of the two flow events over the bed and a preferential presence of one of the two types, which would result in higher spatially-averaged turbulence intensities. Clearly, the mechanisms by which fluid is exchanged between the bed and the overlying flow, and the spatial distribution of this exchange is likely to be different between screeded and fed beds. This could influence the exchange of soluble and fine particulate pollutants between the pore water and overlying flow.

The bed surface topography results in the previous results section do not support the conclusions made over the levels of spatial variability in $\bar{u}$. It would be expected that a greater bed surface complexity and organization would result in higher levels of spatial variability. However, Cooper and Tait (2008) discovered that the spatial pattern of $\bar{u}$ has little linear coherence with bed surface topography at the grain-scale. Therefore, although surprising, a greater bed surface complexity does not necessarily result in a greater degree of spatial variability in the flow.

DOI: 10.1002/esp

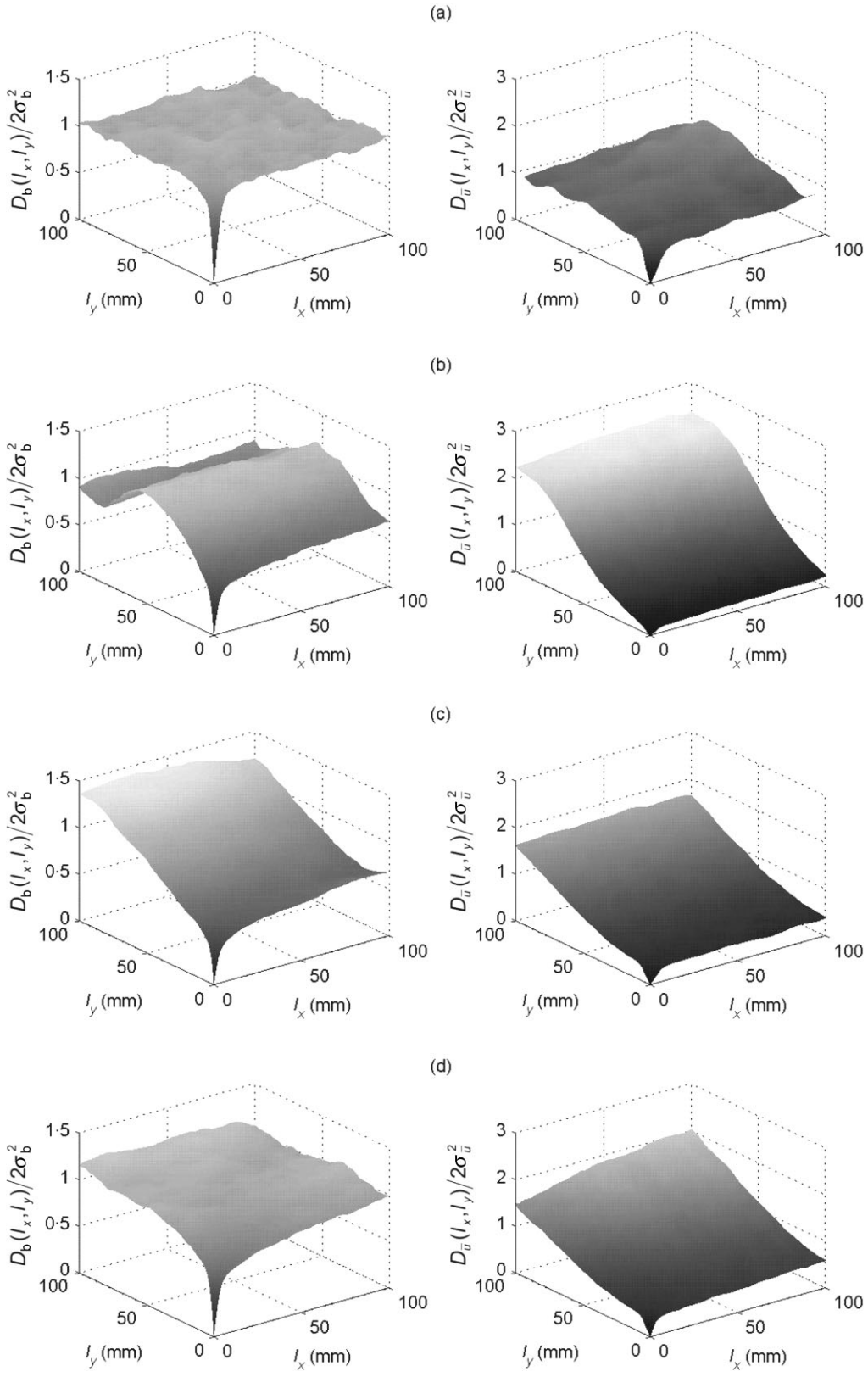

Figure 8. Surface plots of the second-order structure functions D_b of the bed surface elevations normalized by $2\sigma_b^2$ (left) and $D_{\bar{u}}$ of the time-averaged streamwise velocities normalized by $2\sigma_{\bar{u}}^2$ (right) for (a) the screeded bed; (b) fed bed 1; (c) fed bed 2; and (d) fed bed 3.

Figure 8 shows the normalized structure functions $D_{\bar{u}}(l_x,l_y)/2\sigma_{\bar{u}}^2$ of $\bar{u}$ for the four beds, where $\sigma_{\bar{u}}$ is the standard deviation in time-averaged velocities over the bed. This is compared against $D_b(l_x,l_y)/2\sigma_b^2$ for the corresponding bed surfaces. Briefly, it can be seen that the flow over the screeded bed has little correlation in either direction and therefore can be considered almost random in organization (Figure 8a). In contrast, the flow over the three fed beds has strong streamwise coherency at small lateral lags, which extends beyond the streamwise size of the plot (Figure 8b–d). This indicates the presence of long streamwise structures in the flow, most likely to be high-speed streaks (Cooper and Tait, 2008). These structures do not appear to have a single dominant lag in the lateral direction and the lateral correlation becomes negligible at small lateral lags, indicating that the flow structures are relatively narrow.

DOI: 10.1002/esp

The similarity in the surfaces of the structure functions of z_b and $\bar{u}$ suggest that, although the linear correlation between z_b and $\bar{u}$ maybe poor at the grain-scale, the correlation may be improved at large scales, such as the scales of large bed surface structures. It reveals that the greater bed surface complexity and organization of the fed beds results in a higher degree of organization in $\bar{u}$. However, the difference in bed surface topography between the screeded and fed beds is not reflected in the values of $\sqrt{\langle \tilde{u}^2 \rangle}/u_*$, $Sk_{\tilde{u}}$ and $Ku_{\tilde{u}}$. This shows that the statistical measures of the distribution of time-averaged streamwise velocity are not able to adequately discriminate the differences in flow organization between the four beds. These measures do not carry any 'directional' information, and therefore are not capable of representing the geometrical properties of the flow associated with the different orientations of flow structures. They therefore fail to provide a reliable tool to represent the degree of organization of the flow. It is therefore suggested that structure functions should be employed when comparing the organization of the flow over beds with different surface topographies.

Conclusions

An examination has been made of gravel beds formed in the laboratory using two different methods. The results revealed that the physical properties of beds created through the manual-placement and screeding of sediment were clearly different from those formed through sediment feeding. The screeded bed had a random organization of grains on both the surface and within the subsurface. The fed beds exhibited greater surface and subsurface organization and complexity, and had a number of properties that closely resembled those found for natural water-worked gravel beds: (1) the distributions of the bed surface elevations were positively skewed; (2) the vertical roughness length scales were less than half the horizontal roughness length scales; (3) the majority of the particles and micro-bedforms (imbricated grains) rested on the bed with their *a*-axis in the direction of the flow and their *b*-axis normal to the flow, which along with a positively skewed distribution indicated water-worked, armoured surfaces; (4) preferential particle orientation and direction of imbrication in the subsurface, as well as bulk porosity and hydraulic conductivity values which closely resemble those found in poorly sorted gravel lithofacies of in-channel fluvial deposits. This suggested that fed beds are able to simulate, in a simplified manner, both the surface and subsurface properties of established gravel-bed river deposits in laboratory flumes.

To understand the importance of using fed beds for investigating near-bed river processes, the temporal and spatial characteristics of the near-bed flow field were also compared between the screeded and fed beds. It revealed that the use of a screeded bed will typically cause an underestimation in the turbulence intensities, and as such, in the degree of temporal variability in the flow, in comparison to water-worked fed beds. Furthermore, time-averaged streamwise velocities were found to be randomly organized over the screeded bed but were organized into long streamwise flow structures over the fed beds. It clearly shows that caution should be taken when comparing velocity measurements over screeded beds with water-worked beds.

The differences in the properties of the surface and subsurface of screeded fed beds, and in their near-bed flow conditions, have important consequences for the design of river beds for river restoration projects. These projects often result in the construction of new channels or river beds where the deposits have not (necessarily) been water-worked. The results suggest that this may not be appropriate, and that in order to replicate faithfully the hydraulic and ecological components of an established gravel-bed river, a bed should be constructed that is formed through the sequential cycles of sediment transport and deposition.

Although screeded beds that have been water-worked for a period of time are likely to be able to simulate near-bed flow conditions in the same manner as fed beds, they are unlikely to be suitable for studying sediment–water interface exchange mechanisms, such as the exchange of soluble and fine particulate pollutants between the overlying river flow and the pore water. The formation of fed beds therefore offers an improved way of investigating intragravel flow and exchange processes in gravel-bed rivers at a laboratory scale.

Acknowledgements—The work was completed when J.R.C. was in receipt of a University of Sheffield Project Studentship, and written while in receipt of an ARCO Research Fellowship at the University of Hull. The authors are grateful to Dr Amir Chegini who kindly provided flow data for the screeded bed, and to Dr Jochen Aberle for his assistance in producing Figure 6.

References

Aberle J. 2007. Measurements of armour layer roughness geometry function and porosity. *Acta Geophysica* **55**: 23–32.

Aberle J, Nikora V. 2006. Statistical properties of armored gravel bed surfaces. *Water Resources Research* **42**. DOI: 10.1029/2005WR004674

Aberle J, Smart GM. 2003. The influence of roughness structure on flow resistance on steep slopes. *Journal of Hydraulic Research* **41**: 259–269.

Allen JRL. 1982. *Sedimentary Structures: Their Character and Physical Basis*. Elsevier: Amsterdam.

Barison S, Chegini A, Marion A, Tait SJ. 2003. Modifications in near bed flow over sediment beds and the implications for grain entrainment. *Proceedings of XXX IAHR Congress, Theme C: Turbulence-2*, Thessalonki; 509–516.

Barrash W, Reboulet EC. 2004. Significance of porosity for stratigraphy and textural composition in subsurface, coarse fluvial deposits: Boise Hydrogeophysical Research Site. *Geological Society of America Bulletin* **116**: 1059–1073.

Bear J. 1972. *Dynamics of Fluids in Porous Media*. Dover Publications: New York.

Bergeron NE. 1996. Scale-space analysis of stream-bed roughness in coarse gravel-bed streams. *Mathematical Geology* **28**: 537–561.

Brown A, Willetts B. 1997. Sediment flux, grain sorting and the bed condition. In *Environmental and Coastal Hydraulics: Protecting the Aquatic Habitat*, Vol. 2, Wang SSY, Carstens T (eds). American Society of Civil Engineers: New York; 1469–1474.

Buffin-Bélanger T, Reid I, Rice S, Chandler JH, Lancaster J. 2003. A casting procedure for reproducing coarse-grained sedimentary surfaces. *Earth Surface Processes and Landforms* **28**: 787–796.

Butler JB, Lane SN, Chandler JH. 2001. Characterization of the structure of river-bed gravels using two-dimensional fractal analysis. *Mathematical Geology* **33**: 301–330.

Campbell L, McEwan I, Nikora V, Pokrajac D, Gallagher M, Manes C. 2005. Bed-load effects on hydrodynamics of rough-bed open-channel flows. *Journal of Hydraulic Engineering, American Society of Civil Engineers* **131**: 576–585.

Carling PA, Reader NA. 1982. Structure, composition and bulk properties of upland stream gravels. *Earth Surface Processes and Landforms* **7**: 349–365.

Carman PC. 1937. Fluid flow through granular beds. *Transactions of the Institute of Chemical Engineers* **15**: 150.

Cooper JR. 2006. *Spatially-induced momentum transfer over water-worked gravel beds*. PhD Thesis, University of Sheffield.

Cooper JR, Tait SJ. 2008. The spatial organisation of time-averaged streamwise velocity and its correlation with the surface topography of water-worked gravel beds. *Acta Geophysica* **56**: 614–642.

Dantec. 2000. *FlowMap Particle Image Velocimetry Instrumentation: Installation and Users Guide*. Dantec Measurement Technology: Skovlunde.

Diplas P, Sutherland AJ. 1988. Sampling techniques for gravel sized sediments. *Journal of Hydraulic Engineering, American Society of Civil Engineers* **114**: 484–501.

Dittrich A, Koll K. 1997. Velocity field and resistance of flow over rough surface with large and small relative submergence. *International Journal of Sediment Research* **12**: 21–33.

Ferro V. 2003. ADV measurements of velocity distributions in a gravel-bed flume. *Earth Surface Processes and Landforms* **28**: 707–722.

Goring DG, Nikora VI, McEwan IK. 1999. Analysis of the texture of gravel beds using 2-D structure functions. *Proceedings of IAHR Symposium on River, Coastal and Estuarine Morphodynamics*, Genova; 111–120.

Heinz J, Kleineidam S, Teutsch G, Aigner T. 2003. Heterogeneity patterns of Quaternary glaciofluvial gravel bodies (SW-Germany): application to hydrogeology. *Sedimentary Geology* **158**: 1–23.

Komura S. 1963. Discussion of 'Sediment transportation mechanics: introduction and properties of sediment'. *Journal of the Hydraulics Division, ASCE* **89**: 263–266.

Kostic B, Becht A, Aigner T. 2005. 3-D sedimentary architecture of a Quaternary gravel delta (SW-Germany): implications for hydro-stratigraphy. *Sedimentary Geology* **181**: 147–171.

Kozeny J. 1927. *Über die kapillare Leitung des Wassers im Boden*. Akademie der Wissenschaften: Wien.

Lawless M, Robert A. 2001. Scales of boundary resistance in coarse-grained channels: turbulent velocity profiles and implications. *Geomorphology* **39**: 221–238.

Lisle TE, Lewis J. 1992. Effects of sediment transport on survival of salmonid embryos in a natural stream: a simulation approach. *Canadian Journal of Fisheries and Aquatic Sciences* **449**: 2337–2344.

Marion A, Fraccarollo L. 1997. New conversion model for areal sampling of fluvial sediments. *Journal of Hydraulic Engineering, American Society of Civil Engineers* **123**: 1148–1151.

Marion A, Tait SJ, McEwan IK. 2003. Analysis of small-scale gravel bed topography during armoring. *Water Resources Research* **39**. DOI: 10.1029/2003WR002367

Meyer-Peter E, Müller R. 1948. Formulas for bed-load transport. *Proceedings of 2nd Congress of IAHR*, Stockholm; 39–64.

Milhous RT. 2001. Specific weight and median size of the bed material of gravel and cobble rivers. *Proceedings of the Seventh Federal Interagency Sedimentation Conference* **1**: III70–III77.

Nezu I, Nakagawa H. 1993. *Turbulence in Open Channel Flows*. A. A. Balkema: Rotterdam.

Nikora V, Walsh J. 2004. Water-worked gravel surfaces: high-order structure functions at the particle scale. *Water Resources Research* **40**. DOI: 10.1029/2004WR003346

Nikora VI, Goring DG, Biggs BJF. 1998. On gravel-bed roughness characterization. *Water Resources Research* **34**: 517–527.

Nikora V, Goring D, McEwan I, Griffiths G. 2001. Spatially averaged open-channel flow over rough bed. *Journal of Hydraulic Engineering, American Society of Civil Engineers* **127**: 123–133.

Packman AI, Marion A, Zaramella M, Chen C, Gaillard J, Keabe DT. 2007. Development of layered sediment structure and its effects on pore water transport and hyporheic exchange. In *The Interactions Between Sediments and Water*, Kronvang B, Faganeli J, Ogrinc N (eds). Springer: Amsterdam; 69–78.

Paola C, Parker G, Seal R, Sinha SK, Southard JB, Wilcock PR. 1992. Downstream fining by selective deposition in a laboratory flume. *Science* **258**: 1757–1760.

Parker G, Toro-Escobar CM, Ramey M, Beck S. 2003. Effect of floodwater extraction on mountain stream morphology. *Journal of Hydraulic Engineering, American Society of Civil Engineers* **129**: 885–895.

Peakall J, Ashworth P, Best J. 1996. Physical modelling in fluvial geomorphology: principles, applications and unresolved issues. In *The Scientific Nature of Geomorphology*, Rhoads BL, Thorn CR (eds). Wiley: Chichester; 221–253.

Robert A. 1988. Statistical properties of sediment bed profiles in alluvial channels. *Mathematical Geology* **20**: 205–225.

Robert A. 1991. Fractal properties of simulated bed profiles in coarse-grained channels. *Mathematical Geology* **23**: 367–382.

Salehin M, Packman AI, Paradis M. 2004. Hyporheic exchange with heterogeneous streambeds: laboratory experiments and modeling. *Water Resources Research* **40**. DOI: 10.1029/2003WR002567

Sambrook Smith GH, Nicholas AP. 2005. Effect on flow structure of sand deposition on a gravel bed: results from a two-dimensional flume experiment. *Water Resources Research* **41**. DOI: 10.1029/2004WR003817

Schmeeckle MW, Nelson JM, Shreve RL. 2007. Forces on stationary particles in near-bed turbulent flows. *Journal of Geophysical Research-Earth Surface* **112**. DOI: 10.1029/2006JF000536

Seal R, Paola C, Parker G, Southard JB, Wilcock PR. 1997. Experiments on downstream fining of gravel: 1. narrow-channel runs. *Journal of Hydraulic Engineering, American Society of Civil Engineers* **123**: 874–884.

Shvidchenko AB, Pender G. 2001. Macroturbulent structure of open-channel flow over gravel beds. *Water Resources Research* **37**: 709–719.

Siegenthaler C, Huggenberger P. 1993. Pleistocene Rhine gravel: deposits of a braided river system with dominant pool preservation. In *Braided Rivers*, Best J, Bristow CS (eds). Special Publication 75, Geological Society Publishing House: Bath; 147–162.

Smart G, Aberle J, Duncan M, Walsh J. 2004. Measurement and analysis of alluvial bed roughness. *Journal of Hydraulic Research* **42**: 227–237.

Smith SA. 1990. The sedimentology and accretionary styles of an ancient gravel-bed stream – the Budleigh Salterton Pebble Beds (Lower Triassic), southwest England. *Sedimentary Geology* **67**: 199–219.

Steel RJ, Thompson DB. 1983. Structures and textures in Triassic braided-stream conglomerates ('Bunter' Pebble Beds) in the Sherwood Sandstone group, North Staffordshire, England. *Sedimentology* **30**: 341–367.

Tait SJ. 1993. *The physical processes of bed armouring in mixed grain sediment transport*. PhD Thesis, University of Aberdeen.

Tait SJ, Willetts BB, Gallagher MW. 1996. The application of Particle Image Velocimetry to the study of coherent flow structures over a stabilizing sediment bed. In *Coherent Flow Structures in Open Channels*, Ashworth PJ, Bennett SJ, Best JL, McLelland SJ (eds). Wiley: Chichester; 184–201.

Toro-Escobar CM, Paola C, Parker G, Wilcock PR, Southard JB. 2000. Experiments on downstream fining of gravel: II. wide and sandy runs. *Journal of Hydraulic Engineering, American Society of Civil Engineers* **126**: 198–208.